

Dolutegravir Derivatives Alleviate LPS-Induced Microglial Inflammation by Suppressing STAT1/3 Nuclear Translocation

Lan Wang¹, Xiaoting Zhang¹, Yimian Wang¹, Longfei Mao¹, Xixi Hou², Lizeng Peng³

¹College of Basic Medicine and Forensic Medicine, Henan University of Science and Technology, Luoyang, 471000, People's Republic of China; ²The First Affiliated Hospital, and College of Clinical Medicine of Henan University of Science and Technology, Luoyang, 471000, People's Republic of China; ³Key Laboratory of Novel Food Resources Processing Ministry of Agriculture, Key Laboratory of Agro-Products Processing Technology of Shandong Province, Institute of Agro-Food Science and Technology, Shandong Academy of Agricultural Sciences, Jinan, 250000, People's Republic of China

Correspondence: Lizeng Peng, Key Laboratory of Novel Food Resources Processing Ministry of Agriculture, Key Laboratory of Agro-Products Processing Technology of Shandong Province, Institute of Agro-Food Science and Technology, Shandong Academy of Agricultural Sciences, Jinan, 250000, People's Republic of China, Email penglizeng@sdnu.edu.cn; Xixi Hou, The First Affiliated Hospital, and College of Clinical Medicine of Henan University of Science and Technology, Luoyang, 471000, People's Republic of China, Email lucyfly881104@163.com

Purpose: Microglial inflammation plays a significant role in a variety of neurological disorders. Dolutegravir as a antiretroviral drug has been reported to inhibit the secretion of pro-inflammatory cytokines. Meanwhile, compounds containing 1,2,3-triazole have shown potential anti-inflammatory properties. Therefore, this study aims to investigate the anti-inflammatory potential of dolutegravir-1,2,3-triazole structural derivatives and elucidate its associated mechanisms of action.

Methods: Dolutegravir-1,2,3-triazole derivatives were synthesized through click chemistry reactions. The anti-inflammatory activity against microglial inflammation and cytotoxicity of these derivatives were evaluated using the Griess assay and MTT assay. In vitro, the effects of the compounds on the expression of inflammatory mediators in LPS-stimulated BV-2 microglial cells were assessed using Real-time PCR, ELISA, and Western blot. In vivo, the effects of the compounds on microglial inflammation and synaptic deficits in the hippocampus of LPS-challenged mice were evaluated using Real-time PCR, immunofluorescence, and Western blot.

Results: We discovered compound **4k** exhibits the best inhibitory effect on microglial inflammation ($IC_{50} = 5.01 \pm 0.57 \mu M$) among the 27 dolutegravir derivatives. Compound **4k** significantly attenuates the expression of LPS-induced microglial M1 phenotype markers, NO, IL-1 β , IL-6, TNF- α , iNOS, and COX-2, while concurrently enhancing the expression of M2 phenotype markers, IL-4 and Ym-1. Further mechanistic exploration has elucidated that compound **4k** modulates the polarization of microglia by suppressing the phosphorylation and nuclear translocation of STAT1/3 proteins. In the hippocampus of LPS-challenged mice, compound **4k** markedly diminishes the expression of the microglial activation marker Iba1 and inflammatory mediators IL-1 β , TNF- α , and COX-2 which led to an enhancement in the expression of the synaptic protein synaptophysin, thereby mitigating the synaptic defects.

Conclusion: Compound **4k** exerts significant anti-microglial inflammatory effects by modulating the STAT signaling pathway to alleviate synaptic defects, which offers promising avenues for developing innovative anti-microglial inflammatory treatment strategies.

Keywords: microglial inflammation, dolutegravir, LPS, STAT signaling pathway

Introduction

Neuroinflammation is an innate physiological reaction elicited by a spectrum of stimuli occurring in the nervous tissues, which is mainly mediated by the activation of microglia, the central nervous system's resident innate immune cells.^{1,2} An exaggerated or chronic neuroinflammatory state, characterized by the continuous secretion of pro-inflammatory mediators, results in synaptic impairments, neuronal degeneration, and cognitive deficits, which potentially participate in neuropathological conditions including Alzheimer's disease, Parkinson's disease, depression, and pain.³⁻⁷

Microglia, the principal innate immune cells of the brain and spinal cord, exert pivotal roles in orchestrating neuroinflammatory processes as well as various neuronal functions, such as immune surveillance and the modulation of neuroplasticity.^{8–10} Under pathological conditions, microglia swiftly adopt an activated state, which can be categorized into two principal phenotypes based on their functional and phenotypic characteristics: the classically activated M1 phenotype and the alternatively activated M2 phenotype.^{11,12} Upon exposure to noxious stimuli like lipopolysaccharide (LPS) or nerve injury, microglial cells undergo M1-type activation, thereby initiating inflammatory cascades. Activated microglial cells overexpress inducible nitric oxide synthase (iNOS) and cyclooxygenase-2 (COX-2), culminating in heightened nitric oxide (NO) synthesis, accompanied by a substantial secretion of pro-inflammatory cytokines, including interleukin-1 β (IL-1 β), interleukin-6 (IL-6) and tumor necrosis factor- α (TNF- α).¹³ However, alternatively activated M2 type microglia generate an array of neuroprotective elements such as interleukin-4 (IL-4), interleukin-10 (IL-10), chitinase-3-like-3 (Chil3, Ym-1 in rodents), Arginase 1 (Arg-1) that serve to mitigate neuronal harm.^{12,14} Given the multifaceted role of microglia, facilitating the polarization of microglia from an M1 to an M2 phenotype could represent a more promising approach in the treatment of neurological diseases.^{15–17}

The STAT signaling pathway can be activated by cytokines, growth factors, or inflammatory stimuli such as LPS. Upon LPS stimulation, STAT in the cytoplasm undergoes phosphorylation, dimerization, and nuclear translocation, which initiates the transcription of downstream genes and engages in the inflammatory process.^{18,19} STAT signaling pathway is involved in the regulation of the balance between the M1 and M2 polarization states of microglia. Furthermore, several studies have shown that modulating the STAT signaling pathway could facilitate the transition of microglia from an M1 to an M2 polarization state.^{17,20,21}

Dolutegravir, a highly active integrase inhibitor of the human immunodeficiency virus (HIV), belongs to first-line antiretroviral drugs with good safety.²² Dolutegravir has demonstrated anti-inflammatory properties, as evidenced by its capacity to suppress the secretion of pro-inflammatory cytokines and adhesion molecules, specifically IL-6, interleukin-8 (IL-8), soluble intercellular adhesion molecule-1 (sICAM-1), and soluble vascular cell adhesion molecule-1 (sVCAM-1) by inhibiting NF- κ B signaling pathway in human coronary artery endothelial cells.²³

A 1,2,3-triazole scaffold is renowned within the realm of nitrogen-containing heterocycles for its versatility in interacting with various biological targets through the formation of diverse non-covalent bonds.²⁴ The unique characteristics of the 1,2,3-triazole scaffold enable it to mimic various functional groups, rendering it a valuable bioisostere in drug discovery endeavors.^{24–26} Previous studies have demonstrated that 1,2,3-triazole-containing compounds could possess anti-inflammatory potential.^{27–29} It was reported that 1,2,3-triazole substituted N-phenyl nitrene derivatives exhibited significant inhibition of IL-1 β secretion in THP1 monocytes.²⁷ In addition, 1,2,3-triazole tethered indole-3-glyoxamide derivatives had significant anti-inflammatory activity by targeting COX-2.²⁸ According to the report, the anti-inflammatory activity of hesperetin was improved by introducing 1,2,3-triazole.²⁹ Therefore, the modification with the 1,2,3-triazole group represents a highly promising strategy for the advancement of innovative therapeutics targeted at neuroinflammation.

Therefore, we utilized the structure of dolutegravir as a parent nucleus and introduced a 1,2,3-triazole group through a click reaction to obtain 27 structural derivatives. Through evaluating the anti-microglial inflammatory activity of 27 structural derivatives, we found that compound **4k** had the most potent inhibitory effects. Consequently, this research focused on a series of in vitro and in vivo evaluations of the anti-microglial inflammatory activity of compound **4k**, as well as its impact on the M1/M2 polarization phenotype of microglia via the STAT signaling pathway, and further discovered its ability to attenuate LPS-induced neuroinflammation.

Materials and Methods

General Procedure for the Preparation of Compound 4a–4m and 5a–5n

The synthesis route was shown in Figure 1 and substituents tabulated in Table S1. Compound 1 (0.3 g, 1 mmol), 3-aminophenylacetylene (0.14 g, 1.2 mmol), HATU (0.57 g, 1.5 mmol), DIPEA (0.39 g, 3 mmol), and DMF (50 mL) were introduced to a 100 mL reaction flask and stirred under nitrogen for 24 hours at room temperature. Upon completion, the light brown reaction mixture was poured into 50 mL of water, causing a solid to precipitate. The solid was filtered, washed, and dried to obtain compound 2.

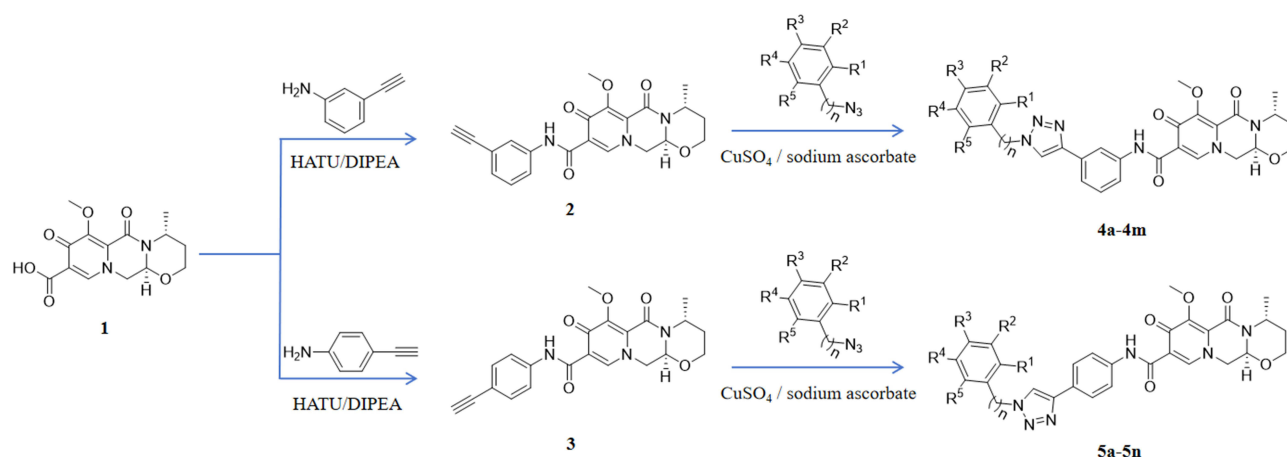


Figure 1 Synthesis route of compound 4a-4m and 5a-5n. Utilizing compound 1 (1 is for compound 1) as the initial reagent, condensation with 3-aminophenylacetylene in the presence of HATU and DIPEA, producing the terminal alkyne compound 2 (2 is for compound 2). The reaction of compound 2 with a substituted azide in a solvent system containing tert-butanol, water, tetrahydrofuran (THF), anhydrous copper sulfate, and sodium ascorbate yielded compounds 4a-4m. Using an analogous procedure, compound 1 was condensed with 4-aminophenylacetylene in the presence of HATU and DIPEA to generate compound 3, which subsequently underwent reaction with diversely substituted azides to furnish compounds 5a-5n.

Subsequently, in a flask, compound 2 (3 mmol), a substituted azide (3.6 mmol), tert-butanol (70 mL), water (70 mL), tetrahydrofuran (70 mL), anhydrous copper sulfate (1.2 g, 6 mmol), and sodium ascorbate (0.36 g, 1 mmol) were sequentially added. The mixture was stirred and refluxed at 70°C for 6 hours. After the reaction, the mixture was extracted with 100 mL dichloromethane three times. Then the organic phase was combined and washed with 100 mL saturated sodium chloride solution twice and then with 100 mL brine twice. The organic phase was dried using sodium sulfate, and the solvent was removed under reduced pressure to yield the crude product. Recrystallization from ethyl acetate provided the desired compound, which was of sufficient purity for further characterization and biological studies.

The method was also suitable for the preparation of compounds 5a-5n. The structural characterization of Compound 4a-4m and 5a-5n was provided in [supplementary information](#).

Cell Culture

BV-2 microglia cells, from Shanghai Institute of Materia Medica, were cultured in flask with DMEM high-glucose medium (LifeTech, Grand Island, NY, USA) containing 10% fetal bovine serum (Gibco, Grand Island, NY, USA) in a humidified, 37 °C and 5% CO₂-containing incubator.

Animals

Male C57BL/6J mice (8–10 weeks old) and Kunming mice (KM mice, 8–10 weeks old) obtained from Henan Skbex Biotechnology Co., Ltd were maintained under standard conditions, featuring a 12-hour inverted light/dark cycle and a temperature range of 22–25 °C with unrestricted access to both food and water. All animal experimentation was conducted according to the guidelines and regulations established by the Animal Care and Use Committee of Henan University of Science and Technology, with the approval reference number being HAUST-024-M081001.

Griess Method

Griess method was used to detect the nitrite content in the culture medium. BV-2 cells were plated in a 96-well cell culture plate at a density of 2×10^4 cells per well. After incubation for 24 hours, test compound was added to achieve final concentrations of 5 μM and 10 μM, while the normal control group (Control group) and the model group (LPS group) received equal volume of solvent. Following 2 hours, LPS solution was added to reach a final concentration of 100 ng/mL, while the normal control group (Control group) received an equivalent volume of solvent. After 24 hours, cell culture supernatant from each well was mixed with an equivalent volume of Griess reagent (Beyotime Biotechnology Co., Ltd. Shanghai, China). The optical density (OD) was detected by a microplate reader (BioTek Instruments, Inc., Winooski, VT, USA) at a wavelength of 540 nm. Concurrently, a standard curve was constructed using sodium nitrite as

the standard, and the nitrite content in the culture medium was calculated based on this standard curve. The raw data for nitrite content in LPS-treated groups was provided in [Table S2](#).

Enzyme-Linked Immunosorbent Assay (ELISA)

The conditioned culture supernatants were collected from BV-2 cells and centrifuged to remove cellular debris, then processed according to the manufacturer's instructions for the ELISA kits specific to IL-6 or TNF- α (Novus Biologicals, CO, USA). Briefly, 50 μ L of sample diluent was added to the microplate wells coated with antibodies, followed by the addition of 50 μ L of the test sample that had been diluted in the same proportion. After incubation at room temperature for 2 hours, the wells were washed five times with the wash solution on a plate shaker, then 100 μ L of enzyme-linked horseradish peroxidase-conjugated antibody was added and incubated at room temperature for 2 hours. The wells were washed five times, and 100 μ L of substrate was added for color development at room temperature. After 30 minutes, 100 μ L of stop solution was added, and the optical density (OD) was measured at a wavelength of 450 nm by a microplate reader (BioTek Instruments, Inc., Winooski, VT, USA), with correction made using the OD value at 570 nm. Concurrently, a standard curve was constructed using the respective standards diluted in a gradient, and the OD₄₅₀ values were determined following the aforementioned steps. The content of IL-6 or TNF- α in the culture medium was calculated based on this standard curve.

RNA Extraction and Quantitative Real-Time PCR

Trizol (Invitrogen, Carlsbad, CA, USA) was used to collect total RNA according to the manufacturer's instructions. The RNA concentration of each group was measured using a Nano Drop spectrophotometer (Thermo Scientific, Wilmington, DE, USA). Reverse transcription was performed according to the instructions of HiScript III RT SuperMix for qPCR (Vazyme Biotech Co., Ltd, Nanjing, China). The resulting cDNA from the reverse transcription of each group was subjected to quantitative Real-time PCR according to the manufacturer's instructions for the ChamQ Pro Universal SYBR qPCR Master Mix (Vazyme Biotech Co., Ltd, Nanjing, China) using an Applied Biosystems 7500 real-time PCR system (Applied Biosystems, Foster City, CA, USA) under the following conditions: initial denaturation at 95 °C for 30 seconds; followed by 40 cycles of denaturation at 95 °C for 5 seconds, and annealing at 60 °C for 30 seconds, with a melting curve analysis. Relative quantification was performed using the $\Delta\Delta$ CT method with threshold cycle (Ct) values. The sequences of the primers used in the reactions are listed in [Table 1](#).

Western Blot Assay

Total protein of cells or tissue samples was extracted using RIPA lysis buffer (containing 1% protease inhibitor, 1 mM NaF, 1 mM Na₃VO₄, 1 mM PMSF). For nuclear protein extraction, NE-PER™ Nuclear and cytoplasmic extraction reagents (Pierce, Thermo Fisher Scientific, Inc., Rockford, IL, USA) were used based on the manufacturer's instructions. The protein concentration was determined using a BCA protein assay kit. Equal amounts of protein from each group were separated by SDS-PAGE and transferred to a 0.2 μ m nitrocellulose membrane using a wet transfer method. Then,

Table 1 Primer Sequence

Gene	Forward Primer (5' to 3')	Reverse Primer (5' to 3')
IL-6	GGAGGCTTAATTACACATGTT	TGATTCAAGATGAATTGGAT
IL-1 β	GCAACTGTTCTGAACTCAACT	ATCTTTTGGGGTCCGTCAACT
TNF- α	CCCTCACACTCAGATCATCTTCT	GCTACGACGTGGGCTACAG
iNOS	GTTCTCAGCCCAACAATACAAA	GTGGACGGGTCGATGTCAC
COX-2	TTGAAGACCAGGAGTACAGC	GGTACAGTTCATGACATCG
IL4	TCAACCCCAAGCTAGTTGTC	TCTCCTGTGACCTCGTTCAA
Ym-1	GAAGGAGCCACTGAGGTCTG	TTGTTGTCCTTGAGCCACTG
Arg-1	GACCTGGCCTTTGTTGATGT	CCATTCTTCTGGACCTCTGC
GAPDH	GGTGAAGGTCGGTGTGAACG	GGTAGGAACACGGAAGGCCA

the membrane was then blocked with 5% non-fat dry milk or bovine serum albumin (BSA) solution at room temperature for 1 hour. After that, the membrane was incubated with the primary antibody solution overnight at 4 °C. The next day, the membrane was washed three times with TBST buffer for 10 minutes each on a shaking bed, then incubated with the secondary antibody solution (Kangchen Biotechnology, Shanghai, China) at room temperature for 2 hours. After further washing with TBST buffer three times for 10 minutes each, the bands were visualized using an ECL detection reagent on an automatic chemiluminescence image analysis system (Shanghai Tanon Science and Technology, Ltd., Shanghai, China), and the band density was quantified using ImageJ software through the following procedure: Scanned gel images were digitally inverted, followed by systematic selection of standardized rectangular regions of interest (ROIs) encompassing individual bands. Quantitative analysis was performed by determining mean pixel intensity values within the defined ROIs, with background subtraction from adjacent non-band areas implemented for signal normalization.

The antibodies used were as follows: anti-iNOS (1:500, BD Biosciences # 610328), anti-COX-2 (1:1000, CST # 12282), anti-phospho-STAT1 (1:1000, CST # 9167), anti-STAT1 (1:5000, CST # 14994), anti-phospho-STAT3 (1:1000, CST # 9145), anti-STAT3 (1:5000, CST # 30835), anti- β -actin (1:10000, Sigma-Aldrich, # A5441), anti-TBP (1:5000, Proteintech # 66166-1-Ig), anti-Synaptophysin (1:1000, Proteintech # 67864-1-Ig), HRP Goat Anti-Rabbit IgG (H+L) (1:5000, Kangchen Biotechnology, KC-RB-035), HRP Goat Anti-Mouse IgG (H+L) (1:5000, Kangchen Biotechnology, KC-MM-035).

Immunocytochemistry

BV-2 cells were plated in a 24-well cell culture plate with glass coverslips coated with poly-L-lysine (PLL). After treatment, the cells were fixed with 4% paraformaldehyde for 15 minutes and permeabilized in methanol at -20 °C for 10 minutes, followed by three rinses with PBS for 5 minutes each. Subsequently, the cells were blocked with an immunocytochemistry blocking solution for 1 hour. Thereafter, the primary antibody solution was applied, and the coverslips were incubated overnight at 4 °C in a humidified chamber. The following day, the coverslips were washed three times with TBST for 5 minutes each. The appropriate secondary antibody solution was added and incubated at room temperature for 2 hours. The cells were then stained with 1 \times DAPI solution (Beijing Solarbio Science & Technology Co., Ltd., Beijing, China) at room temperature for 10 minutes, washed three times with TBST for 5 minutes each, and mounted with antifade mounting medium (Beyotime Biotechnology Co., Ltd. Shanghai, China). Images were captured using a confocal laser microscope (Nikon, Tokyo, Japan) (63 \times objective lens; green channel: 488 nm laser excitation, 500–550 nm emission) and analyzed with ImageJ software. The nuclear-to-cytoplasmic fluorescence intensity ratio of the target protein was analyzed using ImageJ as follows: Multichannel fluorescent images were separated into nuclear (eg, DAPI) and protein-of-interest channels. Nuclei were segmented via thresholding, binary processing, and watershed separation, generating nuclear regions of interest (ROIs). The mean fluorescence intensity of the target protein within nuclear ROIs was quantified. Cytoplasmic ROIs were defined by nuclear area subtraction from whole cells' ROIs. After measuring cytoplasmic fluorescence intensity, the cytoplasmic/nuclear ratio was calculated.

The antibodies used were as follows: anti-phospho-STAT1 (1:100, CST # 9167), anti-phospho-STAT3 (1:100, CST # 9145), CoraLite488-conjugated Goat Anti-Rabbit IgG (H+L) (1:200, Proteintech, SA00013-2).

LPS-Induced Inflammation Animal Model

Male C57BL/6J mice (6–8 weeks old) were randomly assigned to the following groups: Vehicle control group, LPS (Sigma-Aldrich, St Louis, MO, USA, 5 mg/kg, i.p.) group, and LPS+ compound **4k** (10 mg/kg, i.p.) group (n = 5 per group). The mice in compound **4k** treated group received daily intraperitoneal (i.p.) injections of compound **4k** at a dose of 10 mg/kg, while the other groups received an equivalent volume of vehicle (5% DMSO + 40% PEG300 + 1% Tween 80 + 54% saline) for two consecutive days. On the second day, one hour after the administration, the LPS and LPS+ compound **4k** groups were given an intraperitoneal injection of LPS at a dose of 5 mg/kg, whereas the Vehicle group received an equivalent volume of saline. Twenty-four hours after LPS treatment, the mice were anesthetized and perfused for brain collection. The right hemisphere of the brain was fixed in 4% paraformaldehyde for subsequent sectioning and immunofluorescence staining experiments; the hippocampal tissue of the left hemisphere was isolated for biochemical indexes.

Immunofluorescence

The cerebral hemispheres, fixed with 4% paraformaldehyde, were immersed in a gradient series of ethanol, followed by embedding in paraffin. The brain tissues were sectioned into 7-micron-thick slices for subsequent immunofluorescence staining. In brief, the paraffin sections were deparaffinized in xylene for 10 minutes three times and rehydrated through a series of gradient ethanol. Subsequently, the sections were boiled in 10 mM citrate buffer for antigen retrieval for 15 minutes, blocked with immunofluorescence antibody blocking solution for one hour, and then incubated with the corresponding primary antibody solution overnight at 4 °C in a humid chamber. The next day, the sections were incubated with the corresponding secondary antibody solution at room temperature for one hour, followed by rinsing with PBS for three 5-minute intervals. The sections were then treated with an anti-fluorescence quenching agent (Beyotime Biotechnology Co., Ltd. Shanghai, China) and mounted, and images were captured using a fluorescence microscope (Nikon, Tokyo, Japan) (10 × objective lens; green channel: 488 nm laser excitation, 500–550 nm emission) and analyzed with ImageJ software. Quantification of intensity of Iba1 and the number of Iba1+ cells was performed using ImageJ as follows: For intensity quantification, fluorescence images were calibrated using a predefined scale, and ROIs were selected for analysis. Background fluorescence was subtracted by measuring non-cellular areas, and mean fluorescence intensity (MFI) was recorded from 8-bit grayscale-converted images. For positive cell counting, threshold segmentation was applied to generate binary masks, followed by particle analysis with size and circularity filters.

The antibodies used were as follows: anti-Iba1 (1:100, Wako # 019–19741), CoraLite488-conjugated Goat Anti-Rabbit IgG (H+L) (1:200, Proteintech, SA00013-2).

Acute Toxicity Test

Eight-week-old KM mice were assigned to the following groups at random: compound **4k** group (female), solvent control group (vehicle group, female), compound **4k** group (male), and solvent control group (vehicle group, male). The mice in the compound **4k** group received a single gavage of 250 mg/kg compound **4k**, whereas the mice in the vehicle group received an equivalent volume of solvent (5% DMSO + 40% PEG300 + 1% Tween 80 + 54% saline). The body weights of the mice were recorded for the full 14-day period. On day 14 after administration, the mice were anesthetized, blood was collected, and then the mice were sacrificed. Representative organs, including the heart, liver, spleen, lungs, and kidneys, were weighed to calculate the organ index (organ index = organ weight/body weight × 100%), and fixed in 10% formaldehyde and paraffin-embedded for histological examination. In addition, the activities of aspartate aminotransferase and alanine aminotransferase in the blood of each mouse were detected in accordance with the instructions of the kits (Nanjing Jiancheng Bioengineering Institute, Nanjing, China).

Statistical Methods

Each experimental group was independently replicated a minimum of three times. Data are presented as the mean ± standard error of the mean (SEM). The Student's *t*-test was employed to determine the statistical significance between two groups. One-way analysis of variance (ANOVA) coupled with Dunnett's multiple comparison test was utilized to ascertain the statistical significance among multiple groups for a single variable. A P-value of less than 0.05 was considered to indicate statistical significance.

Results

Chemistry

Compound 4a-4m and 5a-5n were synthesized as previously described.³⁰ Utilizing (4R)-7-methoxy-4-methyl-6,8-dioxo-3,4,6,8,12,12a-hexahydro-2H-pyrido[1',2':4,5]pyrazino[2,1-b][1,3]oxazine-9-carboxylic acid (compound 1) as the initial reagent, a multi-step synthesis process was initiated. Initially, compound 1 was condensed with 3-aminephenylacetylene in the presence of HATU and DIPEA, producing the terminal alkyne compound 2. Subsequent reactions of compound 2 with various azide compounds with unique substituents, led to the creation of 13 target compounds (compound 4a-4m), as depicted in [Figure 1](#) and substituents tabulated in [Table S1](#). By the same method, 4-aminephenylacetylene was used to

produce compound 5a-5n. The structures of these target compounds were characterized via ^1H and ^{13}C nuclear magnetic resonance (NMR) spectroscopy ([Supplementary Figures S1-S27](#)).

Biological Evaluations

Screening for Anti-Microglial Inflammatory Activity of Dolutegravir Derivatives

Upon exposure to LPS, microglia generates a plethora of inflammatory mediators, including the cytokines NO, IL-6, and TNF- α .³¹ To identify compounds with anti-microglial inflammatory activity, the Griess method was employed to detect the NO content in the supernatants of LPS-induced microglial cells after being treated with compounds. Cell viability has an influence on the determination of NO content, then the 3-[4,5-dimethylthiazol-2-yl]-2,5-diphenyltetrazolium bromide (MTT) was utilized to assess the vitality of BV-2 microglial cells. In [Table 2](#), the inhibitory effects of 27 compounds on NO production and cell viability at concentrations of 1 μM and 10 μM are presented. Resveratrol was used as control, and at 20 μM , it reduced NO levels in the cell supernatant to $44.22 \pm 2.64\%$ of the LPS group ($P < 0.001$). Dolutegravir at 10 μM decreased NO levels to $51.62 \pm 2.47\%$ of the LPS group but exhibited significant cytotoxicity. Among the 27 structural derivatives, we identified (4R)-N-(3-(1-(2-bromophenyl)-1H-1,2,3-triazol-4-yl)phenyl)-7-methoxy-4-methyl-

Table 2 The Inhibitory Effects of Compounds on LPS-Induced NO Production in BV-2 Cells

Compounds	NO Production (% LPS)		Cell Viability (% LPS)	
	1 μM	10 μM	1 μM	10 μM
4a	101.00 \pm 11.33	92.94 \pm 6.90	63.55 \pm 4.70 ^{####}	53.85 \pm 3.38 ^{####}
4b	90.32 \pm 4.57	11.36 \pm 1.08 ^{***}	97.52 \pm 5.51	14.15 \pm 12.35 ^{####}
4c	78.67 \pm 3.88*	42.20 \pm 5.679 ^{***}	110.30 \pm 2.90	69.76 \pm 3.92 ^{####}
4d	70.26 \pm 2.57**	66.04 \pm 6.96**	115.80 \pm 3.64	68.13 \pm 3.81 ^{####}
4e	71.26 \pm 7.42	29.60 \pm 16.60**	101.20 \pm 1.42 [#]	32.92 \pm 14.55 ^{###}
4f	91.35 \pm 4.18	74.50 \pm 10.84	105.00 \pm 0.73 ^{###}	71.06 \pm 0.95 ^{####}
4g	89.13 \pm 2.68*	60.57 \pm 3.01 ^{***}	108.70 \pm 1.92	70.62 \pm 6.29 ^{###}
4h	75.76 \pm 2.22	97.71 \pm 11.27	106.50 \pm 2.09	62.04 \pm 5.68 ^{####}
4i	87.27 \pm 3.50	56.09 \pm 11.79 ^{**}	104.80 \pm 0.70 ^{###}	55.33 \pm 0.73 ^{####}
4j	85.63 \pm 9.32	60.88 \pm 11.23*	106.00 \pm 1.29 ^{###}	48.14 \pm 0.77 ^{####}
4k	61.21 \pm 5.72**	29.97 \pm 7.30 ^{***}	86.70 \pm 19.58	80.62 \pm 13.34
4l	71.34 \pm 5.49	65.87 \pm 11.29*	112.70 \pm 3.91	94.51 \pm 9.86
4m	96.57 \pm 6.20	72.89 \pm 7.03*	100.80 \pm 3.80	90.94 \pm 8.37
5a	99.88 \pm 4.40	49.60 \pm 8.64**	106.00 \pm 2.62	98.89 \pm 1.91
5b	87.14 \pm 3.04	81.88 \pm 5.72*	77.06 \pm 3.19 ^{###}	48.20 \pm 3.45 ^{####}
5c	117.20 \pm 10.08	136.40 \pm 6.99*	101.70 \pm 0.65	25.37 \pm 2.50 ^{####}
5d	106.30 \pm 7.29	84.22 \pm 6.11	65.93 \pm 1.41 ^{####}	37.95 \pm 3.06 ^{####}
5e	102.20 \pm 0.27	98.00 \pm 3.17	105.30 \pm 1.73	80.80 \pm 10.21
5f	96.25 \pm 11.00	85.69 \pm 7.91	51.64 \pm 2.06 ^{####}	46.41 \pm 2.31 ^{####}
5g	100.70 \pm 5.35	119.8 \pm 5.56*	68.00 \pm 9.64 [#]	42.14 \pm 1.71 ^{####}
5h	112.10 \pm 1.45	131.10 \pm 28.32	111.10 \pm 0.92 ^{###}	61.42 \pm 2.90 ^{####}
5i	71.13 \pm 14.57	76.48 \pm 9.57	105.00 \pm 2.02	74.04 \pm 6.41 ^{###}
5j	102.30 \pm 7.63	86.16 \pm 5.80	104.00 \pm 1.2	103.20 \pm 4.23
5k	108.80 \pm 2.83	77.87 \pm 10.81	101.10 \pm 0.092	100.00 \pm 2.03
5l	87.68 \pm 8.49	86.31 \pm 20.42	103.20 \pm 2.43	89.34 \pm 5.35
5m	86.08 \pm 4.16*	85.81 \pm 2.19*	103.10 \pm 2.05	100.60 \pm 0.73
5n	95.05 \pm 3.592	67.72 \pm 5.08**	103.40 \pm 2.03	90.75 \pm 6.38
dolutegravir	98.47 \pm 2.91	51.62 \pm 2.47 ^{***}	99.65 \pm 1.60	74.18 \pm 4.45 ^{####}
Resveratrol (20 μM)	44.22 \pm 2.64 ^{***}		89.20 \pm 7.50	

Notes: * $P < 0.05$, ** $P < 0.01$, *** $P < 0.001$ vs the LPS group, # $P < 0.05$, ### $P < 0.01$, #### $P < 0.001$ vs the control group; n = 3.

6,8-dioxo-3,4,6,8,12,12a-hexahydro-2H-pyrido[1',2':4,5]pyrazino[2,1-b][1,3]oxazine-9-carboxamide (compound **4k**) having the most potent anti-microglial inflammatory activity, reducing NO levels to $29.97 \pm 7.30\%$ at $10 \mu\text{M}$ without noticeable cytotoxicity.

Compound **4k** Inhibited the Production of Inflammatory Cytokines in BV-2 Microglial Cells Induced by LPS

To further ascertain the regulatory effect of compound **4k** on the release of LPS-induced inflammatory cytokines in microglia, the levels of the inflammatory mediator including NO, IL-6 and TNF- α were measured. The Griess method was employed to detect NO production in BV-2 microglial cells. Compound **4k** was found to reduce the LPS-induced elevation of nitrite levels in a concentration-dependent manner, and the IC_{50} for compound **4k** in inhibiting NO production was $5.01 \pm 0.57 \mu\text{M}$ (Figure 2A). Therefore, subsequent studies will focus on compound **4k** at concentrations of $5 \mu\text{M}$ and $10 \mu\text{M}$. Utilizing the MTT assay, it was observed that compound **4k**, at final concentrations of $5 \mu\text{M}$ and $10 \mu\text{M}$, did not significantly affect the viability of BV-2 microglial cells, indicating that compound **4k** is non-toxic to microglia at the tested concentrations, as depicted in Figure 2B.

Consistent with the above results, the ELISA test indicated that the levels of pro-inflammatory cytokines IL-6 and TNF- α in the supernatant significantly increased following LPS stimulation, which were concentration-dependently reduced by compound **4k** pretreatment, with IL-6 in the supernatant decreasing to 1698 pg/mL ($P < 0.001$) and 1221 pg/mL

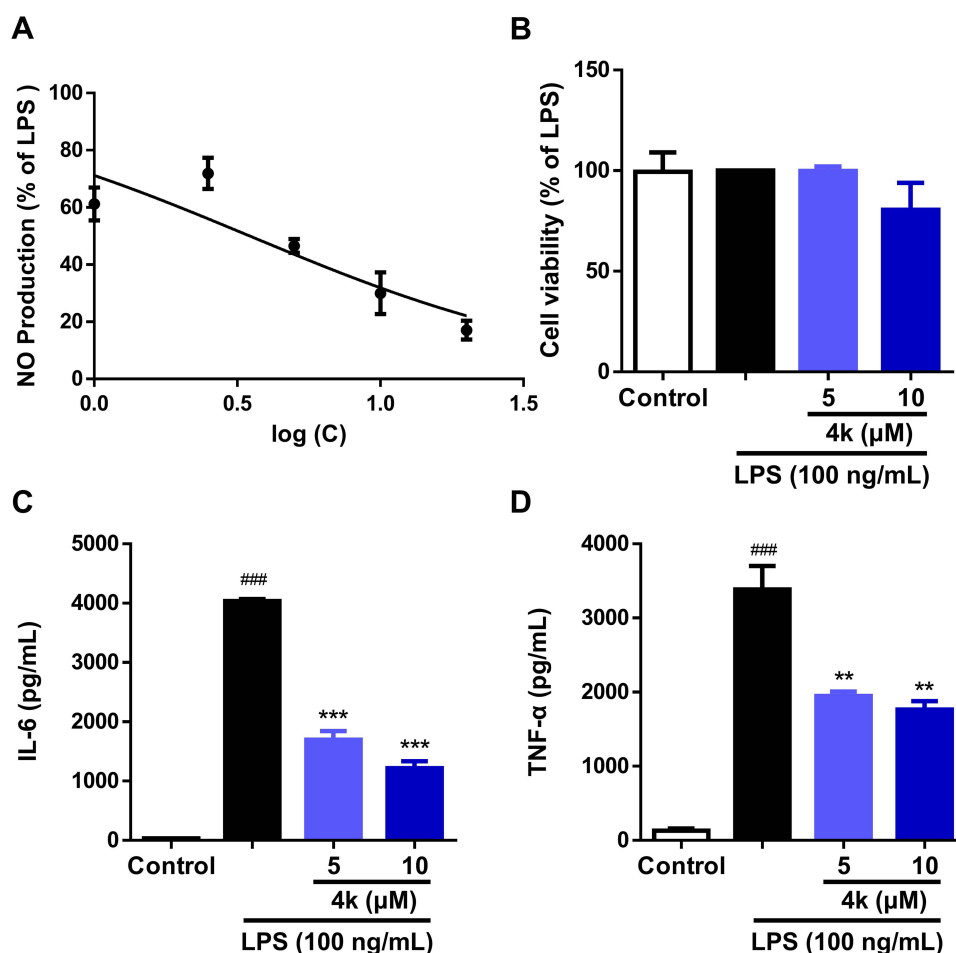


Figure 2 Effect of compound **4k** on the release of LPS-induced inflammatory cytokines in BV-2 microglial cells. (A) BV-2 microglial cells were pretreated with compound **4k** (0, 1, 2.5, 5, 10, and $20 \mu\text{M}$) for 2 h and then exposed to LPS (100 ng/mL) for 24 h. The production of NO was measured using the Griess assay ($n = 3$). BV-2 microglial cells were pretreated with compound **4k** (5, and $10 \mu\text{M}$) for 2 h and then exposed to LPS (100 ng/mL) for 24 h. (B) Cell viability were measured by MTT ($n = 3$). (C and D) The levels of IL-6 and TNF- α were measured by ELISA ($n = 3$). Statistical comparisons between the control group and the LPS-treated group were analyzed using an unpaired Student's *t*-test, ### $P < 0.001$ vs the control group; Statistics among LPS-treated group and compound **4k**-treated groups performed by one-way ANOVA coupled with Dunnett's multiple comparison test, ** $P < 0.01$, *** $P < 0.001$ vs the LPS-treated group.

mL ($P < 0.001$, Figure 2C) at 5 μM and 10 μM , respectively, with parallel reductions in TNF- α to 1948 pg/mL ($P < 0.01$) and 1765 pg/mL ($P < 0.01$, Figure 2D). This indicates that compound **4k** could dose-dependently decrease the release of LPS-induced inflammatory cytokines IL-6 and TNF- α in BV-2 microglial cells.

Compound 4k Modulates the M1/M2 Polarization of BV-2 Microglial Cells

In order to assess the impact of compound **4k** on the phenotypes of microglia, the mRNA levels of the markers of microglial M1/M2 polarization were examined by quantitative real-time PCR technology. Under LPS treatment, the mRNA levels of M1 markers IL-1 β , IL-6, and TNF- α were significantly upregulated, whereas the mRNA levels of M2 markers IL-4, Ym-1, and Arg-1 were markedly downregulated (Figure 3). By contrast, pre-incubation with compound **4k** reduced the LPS-induced rise in IL-1 β , IL-6, and TNF- α mRNA levels, with a maximum effect at 10 μM (Figure 3A–C). As for M2 markers, compound **4k** notably increased the mRNA levels of IL-4 and Ym1 in LPS-induced BV-2 microglial cells (Figure 3D and E), while no significant effect on the mRNA level of Arg-1 in compound **4k**-treatment groups (Figure 3F). The real-time PCR results demonstrated that compound **4k** suppressed the M1 pro-inflammatory phenotype and promoted the M2 anti-inflammatory phenotype in microglia.

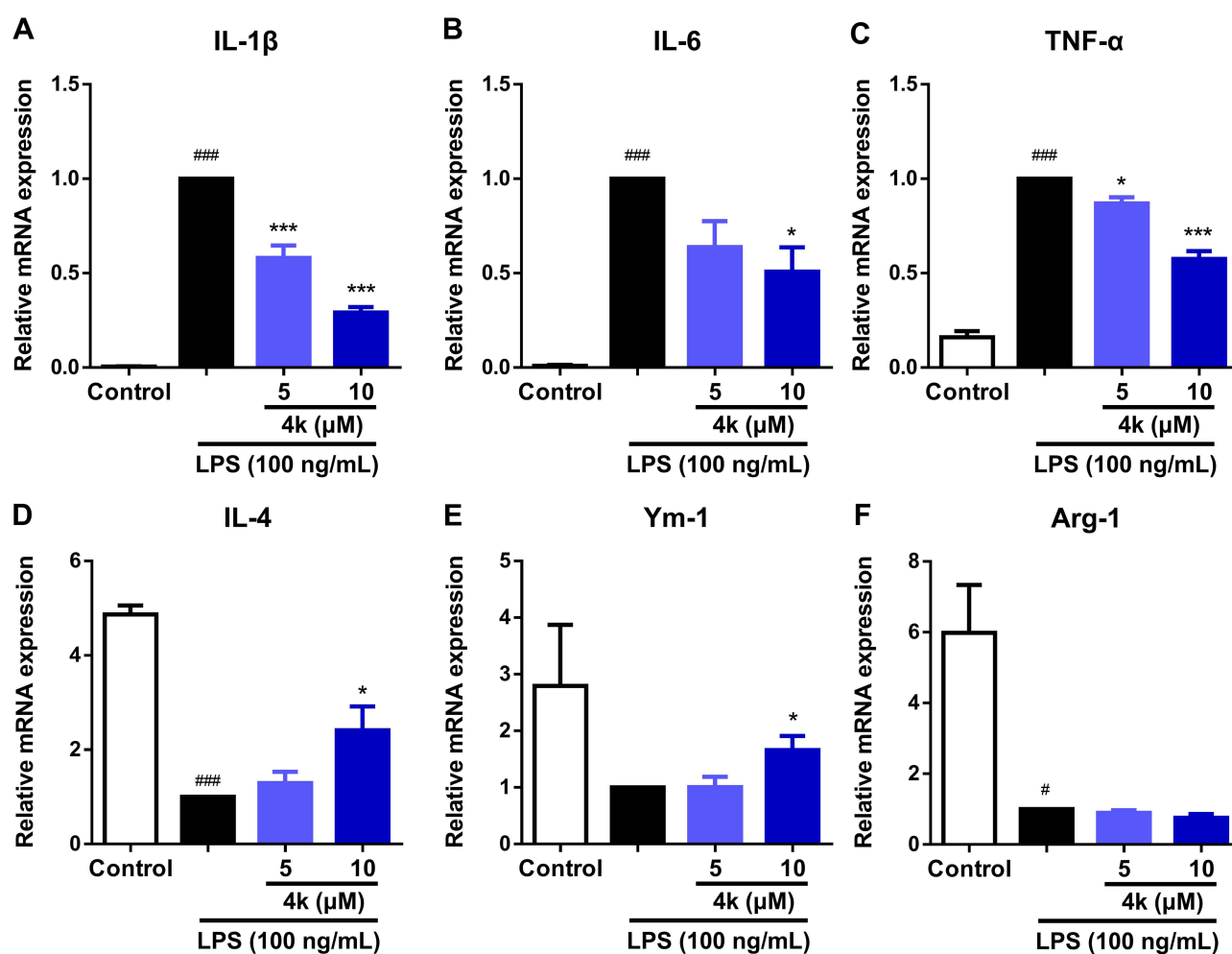


Figure 3 Compound **4k** modulated the M1/M2 polarization of BV-2 Microglial cells. (A–F) BV-2 microglial cells were pretreated with compound **4k** (5, and 10 μM) for 2 h and then exposed to LPS (100 ng/mL) for 6 h. The mRNA levels of M1 markers IL-1 β , IL-6, TNF- α and M2 markers IL-4, Ym-1, Arg-1 were measured by quantitative real-time PCR ($n = 3$). Statistical comparisons between the control group and the LPS-treated group were analyzed using an unpaired Student's *t*-test. # $P < 0.05$, ### $P < 0.001$ vs the control group; Statistics among LPS-treated group and compound **4k**-treated groups performed by one-way ANOVA coupled with Dunnett's multiple comparison test, * $P < 0.05$, *** $P < 0.001$ vs the LPS-treated group.

Compound 4k Reduced the Expression of Pro-Inflammatory Mediators iNOS and COX-2 Induced by LPS in BV-2 Microglia

To further establish the inhibitory activity of compound **4k** on LPS-stimulated microglial inflammation, the transcriptional and protein levels of upstream pro-inflammatory mediators iNOS and COX-2 were assessed using quantitative real-time PCR technology and Western blot analysis, respectively. The results from the real-time PCR demonstrated that compound **4k** significantly attenuated the upregulation of iNOS and COX-2 transcription levels induced by LPS. At a concentration of 5 μM , compound **4k** reduced mRNA levels of iNOS and COX-2 to 77.34% ($P < 0.05$) and 68.01% (vs LPS-treated group), respectively. This suppression was further enhanced at 10 μM , where iNOS and COX-2 mRNA levels decreased to 63.55% ($P < 0.01$, Figure 4A) and 54.15% ($P < 0.05$, Figure 4B). Consistent with the results of

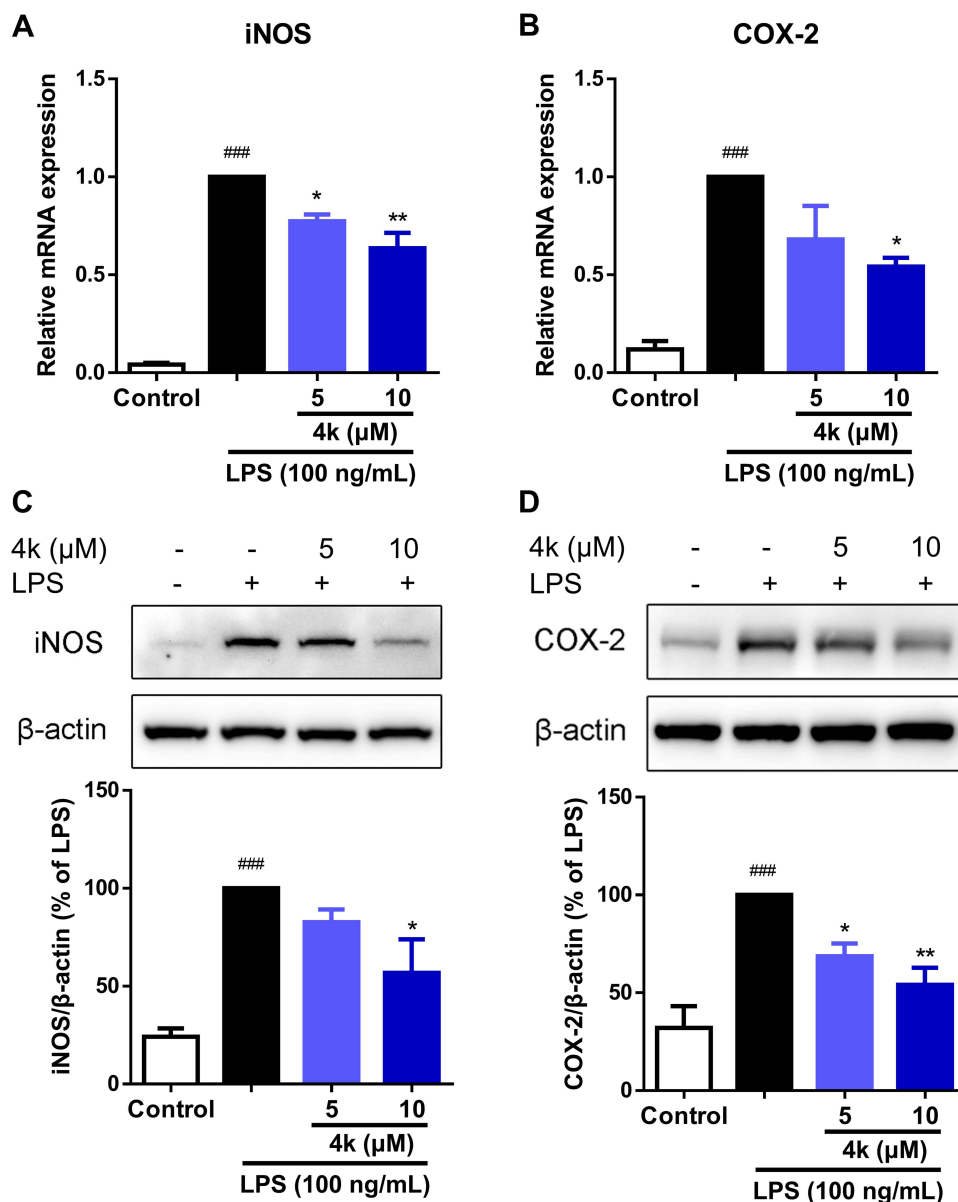


Figure 4 Compound **4k** reduced the expression of pro-inflammatory mediators iNOS and COX-2 in BV-2 Microglial cells. (**A** and **B**) BV-2 microglial cells were pretreated with compound **4k** (5, and 10 μM) for 2 h and then exposed to LPS (100 ng/mL) for 6 h. The mRNA levels of iNOS and COX-2 were measured by quantitative real-time PCR ($n = 3$). (**C** and **D**) BV-2 microglial cells were pretreated with compound **4k** (5, and 10 μM) for 2 h and then exposed to LPS (100 ng/mL) for 24 h. The protein levels of iNOS and COX-2 were measured by Western blot ($n = 3$). Statistical comparisons between the control group and the LPS-treated group were analyzed using an unpaired Student's *t*-test, ### $P < 0.001$ vs the control group; Statistics among LPS-treated group and compound **4k**-treated groups performed by one-way ANOVA coupled with Dunnett's multiple comparison test, * $P < 0.05$, ** $P < 0.01$ vs the LPS-treated group.

transcriptional level, treatment with compound **4k** led to a concentration-dependent decrease in the protein levels of iNOS and COX-2 in BV-2 microglial cells under the influence of LPS (Figure 4C and D).

Compound 4k Reduced LPS-Induced Activation of the STAT Signaling Pathway

The STAT signaling pathway is a crucial mediator in the inflammatory processes of microglia. To elucidate the potential anti-inflammatory mechanism of compound **4k**, the levels of phosphorylation of STAT1 and STAT3 were examined using Western blot analysis. As shown in Figure 5, there was a significant increase in the levels of phosphorylated STAT1 (Tyr701) and STAT3 (Tyr705) following LPS treatment. In contrast, treatment with compound **4k** markedly reduced the LPS-induced elevation of phosphorylated STAT1 ($P < 0.001$ compared to the LPS group, Figure 5A) and phosphorylated STAT3 ($P < 0.01$ compared to the LPS group, Figure 5B). Concurrently, neither LPS nor compound **4k** treatment significantly affected the total protein levels of STAT1/3.

Compound 4k Suppressed LPS-Induced Nuclear Translocation of the Transcription Factor STAT

Upon activation of the JAK/STAT signaling pathway, the transcription factor STATs were phosphorylated and translocated to the nucleus to initiate the transcription of downstream genes.¹⁹ To further verify the regulatory effect of compound **4k** on the LPS-induced JAK/STAT signaling pathway, immunofluorescence and Western blot analysis were employed to examine the impact of compound **4k** on the intracellular distribution of the transcription factor STAT. The immunofluorescence results indicated that exposure to LPS led to an increase in the levels of p-STAT1 within the cell nucleus (Figure 6A and B). However, treatment with compound **4k** significantly reduced the levels of nuclear p-STAT1. We further assessed the nuclear proteins by Western blot analysis. The results were consistent with the aforementioned findings, showing a marked decrease in the levels of phosphorylated STAT1 in the nucleus following compound **4k** treatment (Figure 6C). Meanwhile, we performed immunofluorescence and Western blot analyses to assess the nuclear

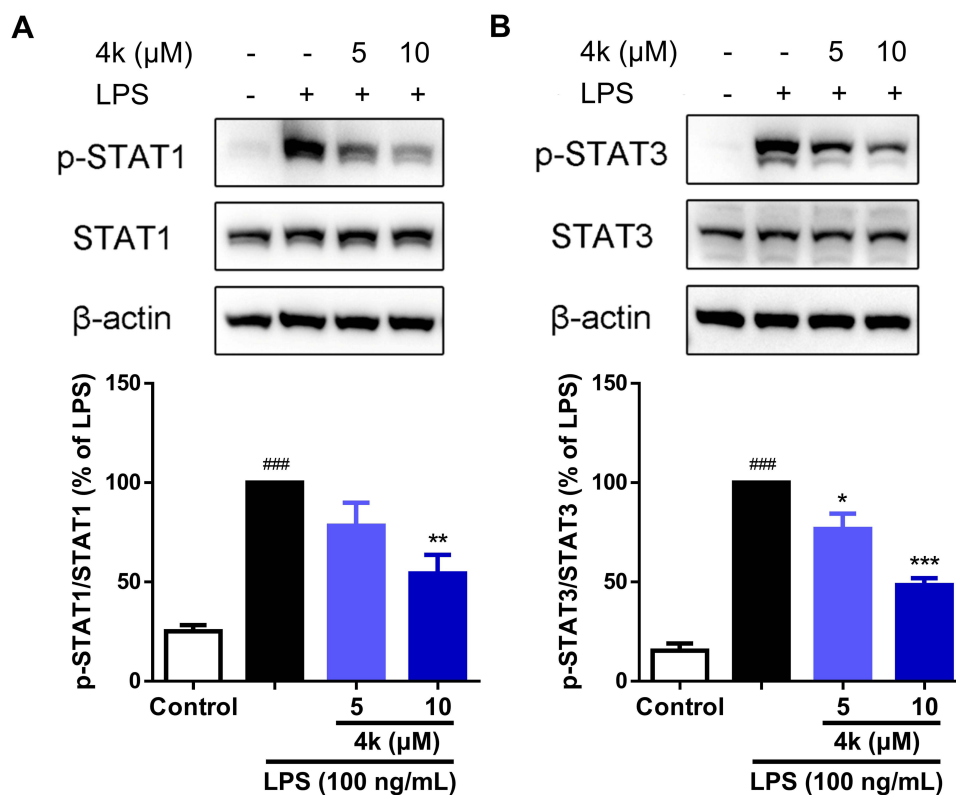


Figure 5 Compound **4k** inhibited the phosphorylation of STAT1/3 in BV-2 Microglial cells. BV-2 microglial cells were pretreated with compound **4k** (5, and 10 μM) for 2 h and then exposed to LPS (100 ng/mL) for 3 h. (A) The protein levels of p-STAT1 and STAT1 were measured by Western blot ($n = 4$). (B) The protein levels of p-STAT3 and STAT3 were measured by Western blot ($n = 4$). Statistical comparisons between the control group and the LPS-treated group were analyzed using an unpaired Student's *t*-test, ### $P < 0.001$ vs the control group; Statistics among LPS-treated group and compound **4k**-treated groups performed by one-way ANOVA coupled with Dunnett's multiple comparison test, * $P < 0.05$, ** $P < 0.01$, *** $P < 0.001$ vs the LPS-treated group.

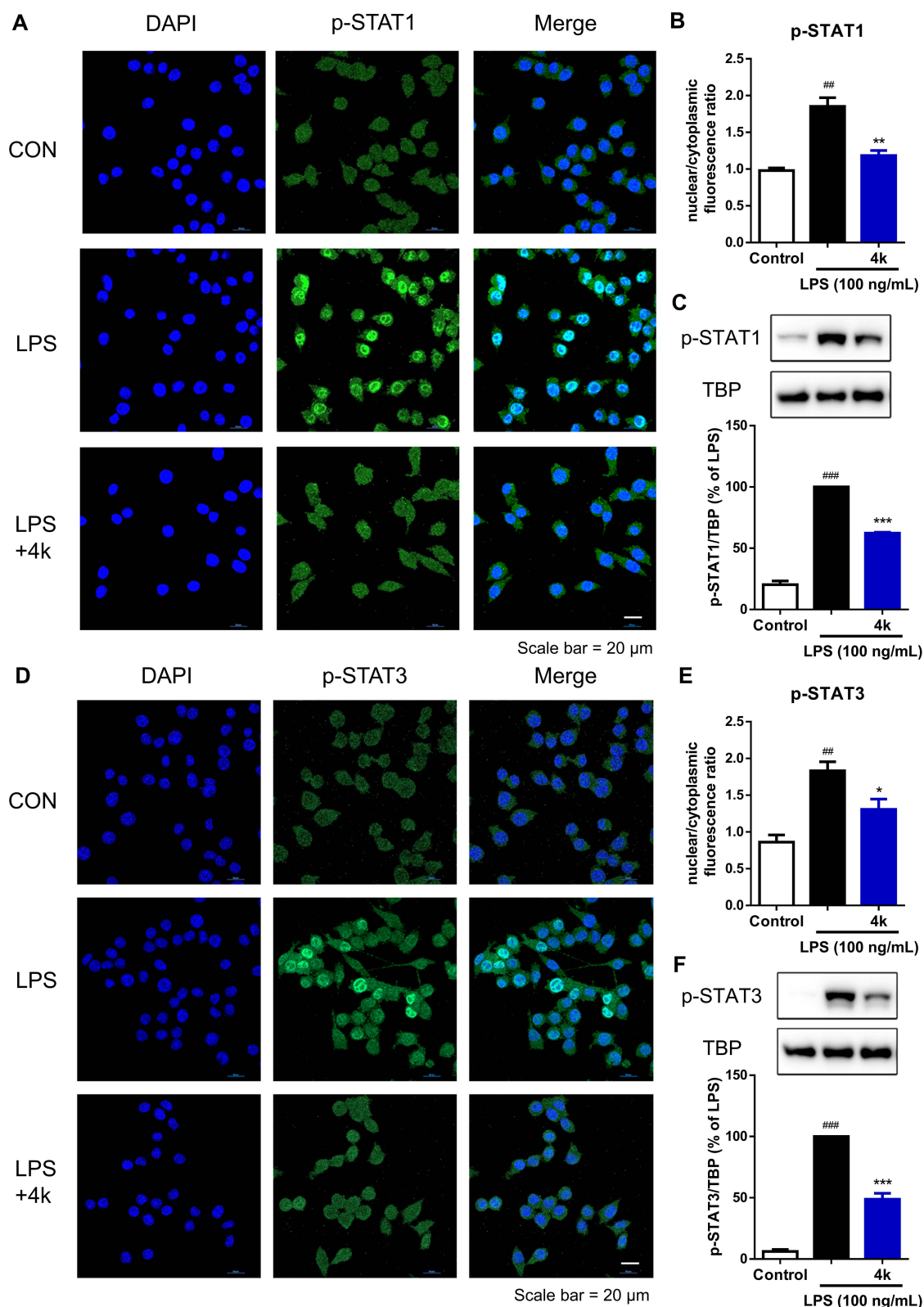


Figure 6 Compound **4k** inhibited the nuclear translocation of STAT1/3 in BV-2 Microglial cells. BV-2 microglial cells were pretreated with compound **4k** (10 μ M) for 2 h and then exposed to LPS (100 ng/mL) for 3 h. (**A** and **D**) The expression and intracellular localization of p-STAT1/3 (green fluorescence) were assessed by immunofluorescence assay (n = 3). Scale bar = 20 μ m. (**B** and **E**) Quantification of nuclear/cytoplasmic fluorescence ratio of p-STAT1/3. (**C** and **F**) The protein level of p-STAT1/3 in the nucleus was measured by Western blot (n = 3). Statistical comparisons between the control group and the LPS-treated group were analyzed using an unpaired Student's *t*-test, ###*P* < 0.01, ####*P* < 0.001 vs the control group; Statistics between LPS-treated group and compound **4k**-treated group performed by an unpaired Student's *t*-test, **P* < 0.05, ***P* < 0.01, ****P* < 0.001 vs the LPS-treated group.

distribution levels of p-STAT3. It was observed that compound **4k** markedly suppressed the LPS-induced upregulation of p-STAT3 levels in the nucleus (Figure 6D–F). These results demonstrate that compound **4k** treatment not only reduced the levels of intracellular p-STAT1/3 following LPS exposure but also effectively decreased their nuclear translocation.

Compound 4k Ameliorates LPS-Induced Microglial Inflammation in the Hippocampus of Mice

We conducted an acute toxicity study in mice to assess the safety profile of compound **4k**. An equal number of male and female mice were observed continuously for 14 days after administration of compound **4k** (250 mg/kg, p.o). The evaluation was performed across several parameters, including body weight, organ indices, pathological changes analysis (H&E staining) and biochemical indicators serum glutamic pyruvic transaminase (GPT), glutamic oxaloacetic transaminase (GOT). The above results indicated that compound **4k** at a dose of 250 mg/kg exhibited no significant toxic effects (Figure 7).

To further assess the *in vivo* anti-microglial inflammatory effects of compound **4k**, the LPS-induced neuroinflammation mice model was used to evaluate the impact of compound **4k** on the status of microglia and levels of inflammatory factors in the hippocampus of mice. After treatment, the mice were anesthetized, perfused, and sacrificed to obtain hemibrains. Then, immunofluorescence staining was conducted utilizing a specific antibody against Iba1 (a marker of activated microglia) to ascertain the activation status of microglia. Following treatment with LPS, the mice exhibit a pronounced neuroinflammatory response with activation and proliferation of microglia. According to the results shown in Figure 8, the upregulated level of Iba1 in the hippocampal region was significantly observed in the LPS group, which was reversed by treatment with compound **4k** (Figure 8A–C).

Activated microglia are associated with pro-inflammatory responses and neuroinflammation.³² The mRNA levels of pro-inflammatory cytokines IL-1 β and TNF- α , as well as the protein level of pro-inflammatory mediator COX-2, in the hippocampus of mice were measured. After exposure to LPS, increased mRNA levels of the pro-inflammatory cytokines IL-1 β and TNF- α were detected by Real-time PCR in the hippocampal region of mice, while co-administration of compound **4k** (10 mg/kg) significantly ameliorated the overproduction of IL-1 β ($P < 0.05$ compared to the LPS group, Figure 8D) and TNF- α ($P < 0.01$ compared to the LPS group, Figure 8E). Consistently, compound **4k** treatment also significantly improved the LPS-induced increase in COX-2 protein levels (Figure 8F and G).

Furthermore, neuroinflammation induces neurotoxicity leading to cell damage and neuronal loss, which in turn causes synaptic dysregulation.³³ Therefore, the protein level of the synaptic protein synaptophysin (SYN) in the hippocampal region was assessed to explore synaptic defects. Western blot results indicated that the protein level of synaptophysin in the hippocampal region significantly decreased under the influence of LPS, which was reversible upon compound **4k** treatment (Figure 8F and H). These findings suggest that compound **4k** could reduce microglial activation, decrease inflammatory factors, and alleviate the synaptic defects in the hippocampal region of mice under LPS-induced stress conditions.

Discussion

In the present study, we have elucidated that: 1) the incorporation of the 1,2,3-triazole moiety into the structure of dolutegravir has yielded 27 dolutegravir structural derivatives; 2) Among 27 dolutegravir structural derivatives, compound **4k** possesses low toxicity and high efficacy against LPS-induced microglial inflammation both *in vitro* and *in vivo*; 3) Compound **4k** suppresses M1-type microglia and promotes the M2 polarization of microglia by inhibiting the STAT signaling pathway; 4) Compound **4k** inhibits the activation of microglia and the expression of inflammatory factors in the hippocampal region, alleviating synaptic deficits.

Dolutegravir has been documented to exhibit anti-inflammatory regulatory effects.^{23,34} Jacqueline Capeau et al reported that dolutegravir mitigates oxidative stress, inflammation, and senescence to improve endothelial dysfunction via suppression of the NF- κ B pathway.³⁴ Additionally, studies indicate that dolutegravir reduces the secretion of pro-inflammatory cytokines IL-6 and IL-8, thereby alleviating inflammatory responses.²³ Consistent with these findings, our experiments demonstrated that dolutegravir at 10 μ M significantly decreased nitric oxide (NO) levels in cell supernatants to $51.62 \pm 2.47\%$ of the LPS-treated group, albeit with concomitant cytotoxicity (Table 2). The 1,2,3-triazole moiety is recognized for its ability to engage in diverse non-covalent interactions with biological targets, conferring multifunctional

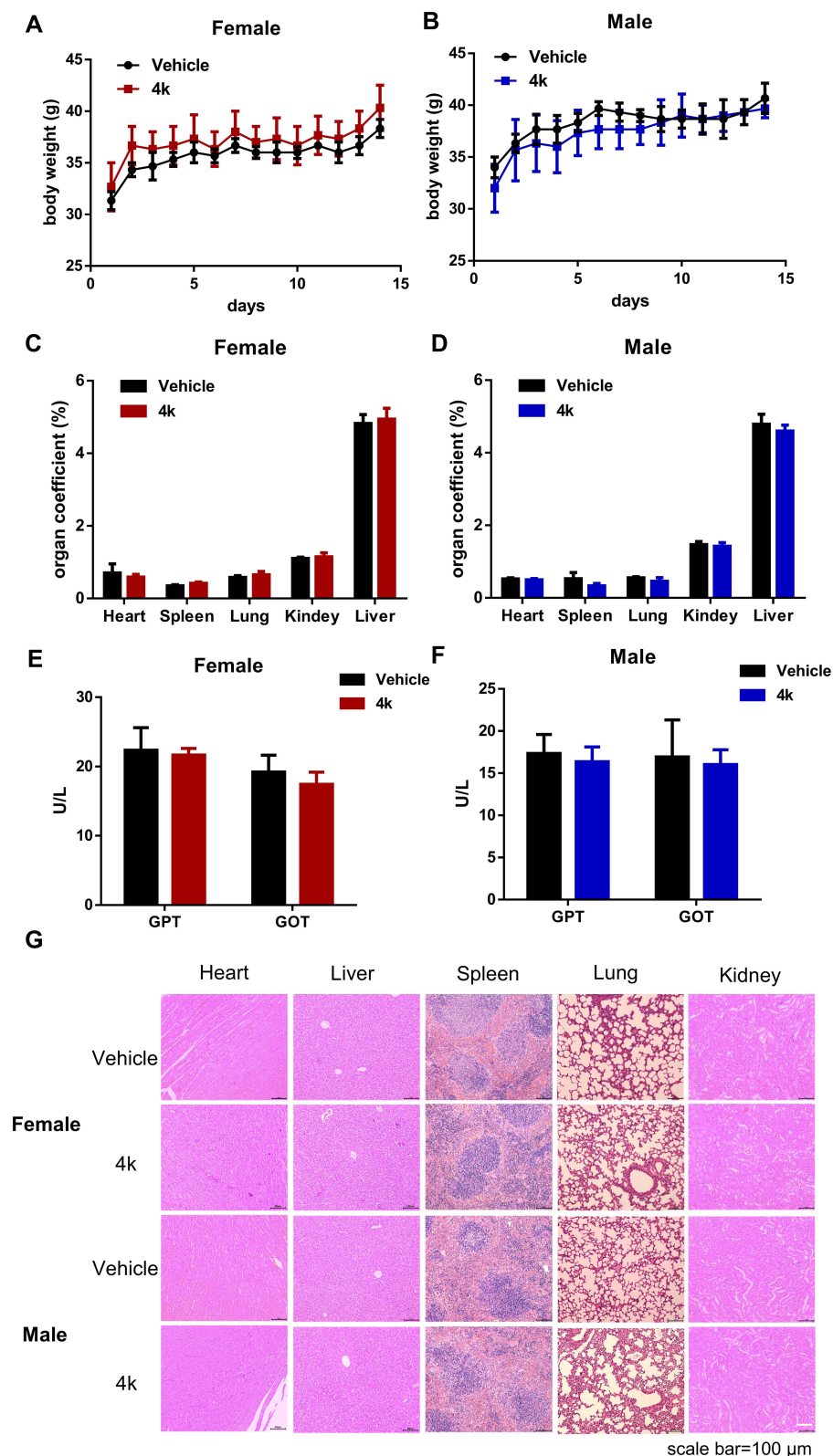


Figure 7 Acute toxicity of compound **4k** with a single oral administration of 250 mg/kg. (**A** and **B**) Body weight after oral administration of 250 mg/kg compound **4k** for 14 days ($n = 3$). (**C** and **D**) The organ coefficient of critical organ on the 14 day after administration ($n = 3$). (**E** and **F**) The levels of GPT and GOT in the plasma of mice ($n = 3$). (**G**) H&E staining were performed on various organs of mice treated with compound **4k**. Scale bar = 100 μm.

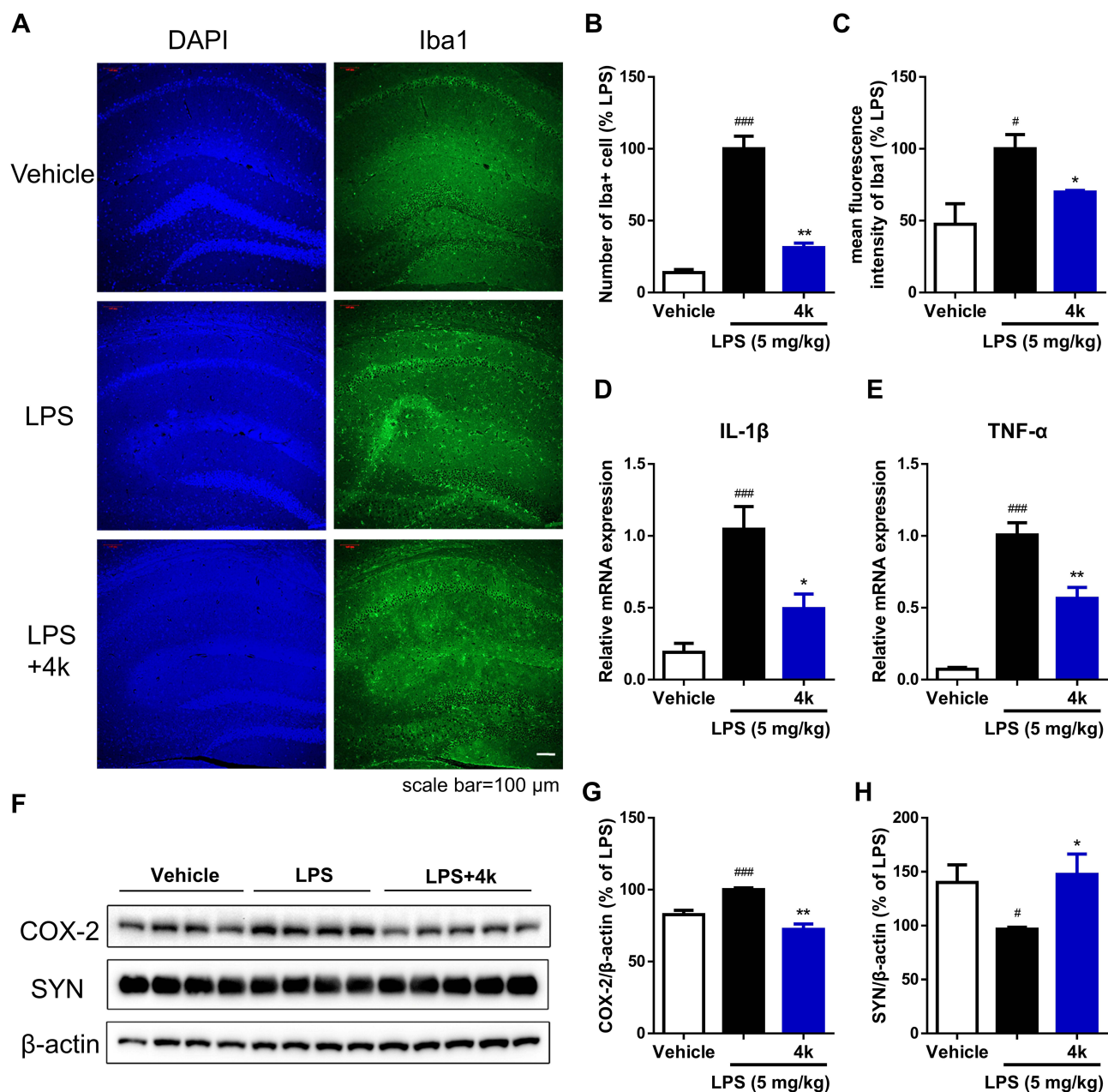


Figure 8 Compound **4k** alleviated LPS-induced activation of microglia and synaptic defects in the hippocampus of mice. Mice were injected with compound **4k** (10 mg/kg, i. p.) or vehicle (5% DMSO + 40% PEG 300 + 1% Tween 80, i.p.) daily for 2 days, followed by injection with LPS (5 mg/kg, i.p.) or saline for 1 day. **(A)** Activation of microglia (Iba1⁺) in the hippocampus was detected by immunofluorescence staining (n = 5). Scale bar = 100 μm. **(B)** Quantification of the number of Iba1⁺ cells in the hippocampus. **(C)** Quantification of mean fluorescence intensity of Iba1. **(D and E)** The mRNA levels of IL-1β and TNF-α in the hippocampus were measured by real-time PCR (n = 5). **(F–H)** The protein level of COX-2 and synaptophysin (SYN) was measured by Western blot (n = 4–5). Statistical comparisons between the Vehicle group and the LPS group were analyzed using an unpaired Student's *t*-test, #*P* < 0.05, ####*P* < 0.001 vs the Vehicle group; Statistics between LPS-treated group and compound **4k**-treated group performed by an unpaired Student's *t*-test, **P* < 0.05, ***P* < 0.01 vs the LPS group.

bioactivities such as anti-inflammatory,^{29,35} anticancer,^{36,37} antimicrobial effects,^{38,39} and so on. In this study, structural modification of dolutegravir with 1,2,3-triazole moiety bearing varied substituents led to significant alterations in anti-inflammatory activity and cytotoxicity. Notably, compound **4k** derived from the conjugation of the dolutegravir core with a triazole moiety via 1,3-position linkage on a benzene ring, exhibited enhanced NO inhibitory activity and reduced cytotoxicity compared to the parent compound. The incorporation of 1,2,3-triazole modifications into dolutegravir significantly enhanced its anti-inflammatory efficacy against LPS-induced microglial inflammation while concurrently reducing cellular toxicity.

Microglia could adopt an activated state by undergoing morphological and phenotypic transformations once cerebral injury and pathological conditions occur.¹⁴ The classical pro-inflammatory (M1) phenotype of microglia is typified by overexpression of pro-inflammatory cytokines and chemokines, while, the alternative anti-inflammatory (M2) phenotype of microglia is characterized by an anti-inflammatory profile that facilitates processes such as repair of nerve injury and the clearance of cellular debris.⁴⁰ In the current study, treatment of compound **4k** suppressed the expression of M1 markers such as IL-1 β , IL-6, TNF- α , iNOS, and COX-2. Conversely, the M2 markers IL-4 and Ym-1 were upregulated in compound **4k**-treated BV-2 microglial cells, which indicated that compound **4k** treatment led to a shift towards an anti-inflammatory M2-like phenotype of microglia.

Increasing evidence showed that interfering STAT signaling pathway could effectively inhibit microglial inflammation by switching the microglia phenotype from M1 to M2.¹² Parthenolide has been demonstrated to attenuate neuroinflammation by modulating microglial polarization via STAT1/3 signaling pathway.⁴¹ In addition, it was found that PLXNA2 knockdown reduced the expression of M1 markers (ie IL-6, IL-1 β , TNF- α , and iNOS) and reversed the low expression of M2 markers (ie CD206, IL-10, and TGF- β), modulating microglia (M1/M2 polarization) to reduce neuroinflammation by inhibiting the activation of STAT3.⁴² In the present study, compound **4k** downregulated LPS-mediated increases in the phosphorylation levels of STAT1/3, and suppressed the nuclear translocation of transcription factor STAT1/3, which indicated that the STAT signaling pathway participates in the regulation of inflammatory responses by compound **4k**.

The concurrent activation of pro-inflammatory markers and the production of cytotoxic factors during neuroinflammatory processes exert deleterious effects on neurons by modulating synaptic protein expression. Neuroinflammation has been demonstrated to reduce the levels of synaptic markers, such as synaptophysin, which mediates the cognitive deficits observed in neurodegenerative and neuropsychiatric disorders.^{43,44} After the LPS challenge, a significant increase in Iba1⁺ microglia levels in the hippocampus of mice was observed, accompanied by high mRNA levels of pro-inflammatory cytokines IL-1 β and TNF- α , corroborating the findings from previous studies.⁴⁵ Moreover, the expression of presynaptic synaptophysin decreased in the hippocampus of LPS-injected mice. However, compound **4k** treatment significantly reduced the levels of Iba1, down-regulated the mRNA levels of TNF- α and IL-1 β , and reversed the LPS-induced synaptic defects of reduced synaptophysin expression. The data suggested that compound **4k** could prevent LPS-induced microglial inflammation and relieve neuron damage by attenuating synaptic defects.

Conclusion

In this study, a series of dolutegravir-1,2,3-triazole structural derivatives were designed and synthesized. Among 27 structural derivatives, compound **4k** shows the most potent suppressive effects on microglial inflammation *in vitro*. Furthermore, compound **4k** exerted an inhibitory effect on the M1 phenotype of microglia, with a reduction of M1 markers including NO, IL-1 β , IL-6, TNF- α , iNOS, and COX-2, while elevating the levels of the M2 marker IL-4 and Ym-1. Compound **4k** facilitated the polarization of microglia towards the M2 phenotype and modulated the M1/M2 polarization balance of microglia through the inhibition of the STAT signaling pathway, thereby effectively mitigating the inflammatory response induced by LPS. Moreover, compound **4k** reduced microglial activation, decreased the overproduction of inflammatory factors IL-1 β and TNF- α , and alleviated the synaptic defects in the hippocampus of C57BL/6J mice subjected to LPS challenge. The study presents robust evidence supporting the therapeutic potential of compound **4k** as an anti-microglial inflammatory agent.

Funding

This study was supported by the Key Scientific Research Projects of Universities in Henan Province (23B310001, 24A350006), International Science and Technology Cooperation Project of Henan Province of China (242102520016).

Disclosure

The authors report no conflicts of interest in this work.

References

- Mary A, Mancuso R, Heneka MT. Immune activation in Alzheimer disease. Annual review of immunology. *Jun.* 2024;42(1):585–613. doi:10.1146/annurev-immunol-101921-035222
- Leng F, Edison P. Neuroinflammation and microglial activation in Alzheimer disease: where do we go from here? *Nat Rev Neurol.* 2021;17(3):157–172. doi:10.1038/s41582-020-00435-y
- Heneka MT, Carson MJ, El Khoury J, et al. Neuroinflammation in Alzheimer's disease. *Lancet Neurol.* 2015;14(4):388–405. doi:10.1016/S1474-4422(15)70016-5
- Kinney JW, Bemiller SM, Murtishaw AS, Leisgang AM, Salazar AM, Lamb BT. Inflammation as a central mechanism in Alzheimer's disease. *Alzheimer's Dementia.* 2018;4:575–590. doi:10.1016/j.trci.2018.06.014
- Hammond TR, Marsh SE, Stevens B. Immune signaling in neurodegeneration. *Immunity.* 2019;50(4):955–974. doi:10.1016/j.immuni.2019.03.016
- Guo BQ, Zhang MY, Hao WS, et al. Neuroinflammation mechanisms of neuromodulation therapies for anxiety and depression. *Transl Psychiat.* 2023;13(1):5. doi:10.1038/s41398-022-02297-y
- Fiore NT, Austin PJ. Are the emergence of affective disturbances in neuropathic pain states contingent on supraspinal neuroinflammation? *Brain Behav Immun.* 2016;56:397–411. doi:10.1016/j.bbi.2016.04.012
- Fourgeaud L, Traves PG, Tufail Y, et al. TAM receptors regulate multiple features of microglial physiology. *Nature.* 2016;532(7598):240–244. doi:10.1038/nature17630
- Hickman S, Izzy S, Sen P, Morsett L, El Khoury J. Microglia in neurodegeneration. *Nat Neurosci.* 2018;21(10):1359–1369. doi:10.1038/s41593-018-0242-x
- Wang Y, Leak RK, Cao G. Microglia-mediated neuroinflammation and neuroplasticity after stroke. *Front Cell Neurosci.* 2022;16:980722. doi:10.3389/fncel.2022.980722
- Subhramanyam CS, Wang C, Hu Q, Dheen ST. Microglia-mediated neuroinflammation in neurodegenerative diseases. *Semin Cell Dev Biol.* 2019;94:112–120. doi:10.1016/j.semdb.2019.05.004
- Long Y, Li XQ, Deng J, et al. Modulating the polarization phenotype of microglia - A valuable strategy for central nervous system diseases. *Ageing Res Rev.* 2024;93:102160. doi:10.1016/j.arr.2023.102160
- Sochocka M, Zwolinska K, Leszek J. The infectious etiology of Alzheimer's disease. *Curr Neuropharmacol.* 2017;15(7):996–1009. doi:10.2174/1570159X15666170313122937
- Zhong X, Gong S, Meng L, et al. Cordycepin modulates microglial M2 polarization coupled with mitochondrial metabolic reprogramming by targeting HKII and PDK2. *Adv Sci.* 2024;11(31):e2304687. doi:10.1002/advs.202304687
- Fan Z, Jia M, Zhou J, et al. Pharmacological targeting cGAS/STING/NF-kappaB axis by tryptanthrin induces microglia polarization toward M2 phenotype and promotes functional recovery in a mouse model of spinal cord injury. *Neural Regen Res.* 2024. doi:10.4103/NRR.NRR-D-23-01256
- Zhao K, Liu J, Sun T, et al. The miR-25802/KLF4/NF-kappaB signaling axis regulates microglia-mediated neuroinflammation in Alzheimer's disease. *Brain Behav Immun.* 2024;118:31–48. doi:10.1016/j.bbi.2024.02.016
- Guo S, Wang H, Yin Y. Microglia polarization from M1 to M2 in neurodegenerative diseases. *Front Aging Neurosci.* 2022;14:815347. doi:10.3389/fnagi.2022.815347
- Ceyzeriat K, Abjean L, Sauvage MA C-D, Ben Haim L, Escartin C. The complex STATes of astrocyte reactivity: how are they controlled by the JAK-STAT3 pathway? *Neuroscience.* 2016;330:205–218. doi:10.1016/j.neuroscience.2016.05.043
- Nabavi SM, Ahmed T, Nawaz M, et al. Targeting STATs in neuroinflammation: the road less traveled! *Pharmacol Res.* 2019;141:73–84. doi:10.1016/j.phrs.2018.12.004
- Lan X, Han X, Li Q, Yang QW, Wang J. Modulators of microglial activation and polarization after intracerebral haemorrhage. *Nat Rev Neurol.* 2017;13(7):420–433. doi:10.1038/nrneuro.2017.69
- Zhou Q, Lin L, Li H, et al. Melatonin reduces neuroinflammation and improves axonal hypomyelination by modulating M1/M2 microglia polarization via JAK2-STAT3-telomerase pathway in postnatal rats exposed to lipopolysaccharide. *Mol Neurobiol.* 2021;58(12):6552–6576. doi:10.1007/s12035-021-02568-7
- Eron JJ, Clotet B, Durant J, et al. Safety and efficacy of dolutegravir in treatment-experienced subjects with raltegravir-resistant HIV type 1 infection: 24-week results of the VIKING study. *J Infect Dis.* 2013;207(5):740–748. doi:10.1093/infdis/jis750
- Auclair M, Guenantin AC, Fellahi S, Garcia M, Capeau J. HIV antiretroviral drugs, dolutegravir, maraviroc and ritonavir-boosted atazanavir use different pathways to affect inflammation, senescence and insulin sensitivity in human coronary endothelial cells. *PLoS One.* 2020;15(1):e0226924. doi:10.1371/journal.pone.0226924
- Bonandi E, Christodoulou MS, Fumagalli G, Perdicchia D, Rastelli G, Passarella D. The 1,2,3-triazole ring as a bioisostere in medicinal chemistry. *Drug Discovery Today.* 2017;22(10):1572–1581. doi:10.1016/j.drudis.2017.05.014
- Deng C, Yan H, Wang J, Liu K, Liu BS, Shi YM. 1,2,3-Triazole-containing hybrids with potential antibacterial activity against ESKAPE pathogens. *Eur J Med Chem.* 2022;244:114888. doi:10.1016/j.ejmech.2022.114888
- Feng LS, Zheng MJ, Zhao F, Liu D. 1,2,3-triazole hybrids with anti-HIV-1 activity. *Arch Pharm.* 2021;354(1):e2000163. doi:10.1002/ardp.202000163
- Sambasiva Rao P, Kurumurthy C, Veeraswamy B, et al. Synthesis of novel 1,2,3-triazole substituted-N-alkyl/aryl nitrene derivatives, their anti-inflammatory and anticancer activity. *Eur J Med Chem.* 2014;80:184–191. doi:10.1016/j.ejmech.2014.04.052
- Naaz F, Preeti Pallavi MC, Shafi S, Mulakayala N, Shahar Yar M, Sampath Kumar HM. 1,2,3-triazole tethered Indole-3-glyoxamide derivatives as multiple inhibitors of 5-LOX, COX-2 & tubulin: their anti-proliferative & anti-inflammatory activity. *Bioorg Chem.* 2018;81:1–20. doi:10.1016/j.bioorg.2018.07.029
- Zheng Y, Zhang YL, Li Z, et al. Design and synthesis of 7-O-1,2,3-triazole hesperetin derivatives to relieve inflammation of acute liver injury in mice. *Eur J Med Chem.* 2021;5(213):113162. doi:10.1016/j.ejmech.2021.113162
- Zhou S, Hou X, Li L, et al. Discovery of dolutegravir-1,2,3-triazole derivatives against prostate cancer via inducing DNA damage. *Bioorg Chem.* 2023;141:106926. doi:10.1016/j.bioorg.2023.106926
- Tang Y, Le W. Differential roles of M1 and M2 microglia in neurodegenerative diseases. *Mol Neurobiol.* 2016;53(2):1181–1194. doi:10.1007/s12035-014-9070-5

32. Zhang M, Chen H, Zhang W, et al. Biomimetic remodeling of microglial riboflavin metabolism ameliorates cognitive impairment by modulating neuroinflammation. *Adv Sci.* 2023;10(12):e2300180. doi:10.1002/advs.202300180
33. Li W, Ali T, He K, et al. Ibrutinib alleviates LPS-induced neuroinflammation and synaptic defects in a mouse model of depression. *Brain Behav Immun.* 2021;92:10–24. doi:10.1016/j.bbi.2020.11.008
34. Afonso P, Auclair M, Caron-Debarle M, Capeau J. Impact of CCR5, integrase and protease inhibitors on human endothelial cell function, stress, inflammation and senescence. *Antiviral Ther.* 2017;22(8):645–657. doi:10.3851/IMP3160
35. Gonzaga DTG, Ferreira LBG, Moreira Marmaldo Costa TE, et al. 1-Aryl-1H- and 2-aryl-2H-1,2,3-triazole derivatives blockade P2X7 receptor in vitro and inflammatory response in vivo. *Eur J Med Chem.* 2017;139:698–717. doi:10.1016/j.ejmech.2017.08.034
36. Wang FC, Peng B, Ren TT, et al. A 1,2,3-triazole derivative of quinazoline exhibits antitumor activity by tethering RNF168 to SQSTM1/P62. *J Med Chem.* 2022;65(22):15028–15047. doi:10.1021/acs.jmedchem.2c00432
37. Gowda SV, Kim NY, Harsha KB, et al. A new 1,2,3-triazole-indirubin hybrid suppresses tumor growth and pulmonary metastasis by mitigating the HGF/c-MET axis in hepatocellular carcinoma. *J Adv Res.* 2024. doi:10.1016/j.jare.2024.08.033
38. Rathinam S, Hjalmsdottir MA, Thygesen MB, Masson M. Chitotriazolol (poly(beta(1-4)-2-(1H-1,2,3-triazol-1-yl)-2-deoxy-d-glucose)) derivatives: synthesis, characterization, and evaluation of antibacterial activity. *Carbohydr Polym.* 2021;267:118162. doi:10.1016/j.carbpol.2021.118162
39. Gadali KE, Rafya M, El Mansouri AE, et al. Design, synthesis, and molecular modeling studies of novel 2-quinolone-1,2,3-triazole-alpha-aminophosphonates hybrids as dual antiviral and antibacterial agents. *Eur J Med Chem.* 2024;268:116235. doi:10.1016/j.ejmech.2024.116235
40. Plastira I, Bernhart E, Goeritzer M, et al. 1-Oleyl-lysophosphatidic acid (LPA) promotes polarization of BV-2 and primary murine microglia towards an M1-like phenotype. *J Neuroinflamm.* 2016;13(1):205. doi:10.1186/s12974-016-0701-9
41. Tao G, Qian D, Li L, et al. Parthenolide promotes the repair of spinal cord injury by modulating M1/M2 polarization via the NF-kappaB and STAT 1/3 signaling pathway. *Cell Death Discovery.* 2020;6(1):97. doi:10.1038/s41420-020-00333-8
42. Li S, Hua X, Zheng M, et al. PLXNA2 knockdown promotes M2 microglia polarization through mTOR/STAT3 signaling to improve functional recovery in rats after cerebral ischemia/reperfusion injury. *Exp Neurol.* 2021;346:113854. doi:10.1016/j.expneurol.2021.113854
43. Rao JS, Kellom M, Kim HW, Rapoport SI, Reese EA. Neuroinflammation and synaptic loss. *Neurochem Res.* 2012;37(5):903–910. doi:10.1007/s11064-012-0708-2
44. Liu Y, Zhang Y, Zheng X, et al. Galantamine improves cognition, hippocampal inflammation, and synaptic plasticity impairments induced by lipopolysaccharide in mice. *J Neuroinflamm.* 2018;15(1):112. doi:10.1186/s12974-018-1141-5
45. Wang L, Zhao D, Wang H, Wang L, Liu X, Zhang H. FPS-ZM1 inhibits LPS-induced microglial inflammation by suppressing JAK/STAT signaling pathway. *Int Immunopharmacol.* 2021;100:108117. doi:10.1016/j.intimp.2021.108117

Drug Design, Development and Therapy

Publish your work in this journal

Drug Design, Development and Therapy is an international, peer-reviewed open-access journal that spans the spectrum of drug design and development through to clinical applications. Clinical outcomes, patient safety, and programs for the development and effective, safe, and sustained use of medicines are a feature of the journal, which has also been accepted for indexing on PubMed Central. The manuscript management system is completely online and includes a very quick and fair peer-review system, which is all easy to use. Visit <http://www.dovepress.com/testimonials.php> to read real quotes from published authors.

Submit your manuscript here: <https://www.dovepress.com/drug-design-development-and-therapy-journal>

Dovepress
Taylor & Francis Group